Adaptive higher order numerical simulation of heat and mass transfer in fluidized beds

Ch. Nagaiah[1] * and G. Warnecke[2] †

1. Institute of Mathematics and Scientific Computing, University of Graz,
Heinrichstr. 36, A-8010 Graz, Austria.

2. Institute of Analysis and Numerics, Otto-von-Guericke University,
Universitätsplatz 2, D-39106 Magdeburg, Germany

October 9, 2008

Abstract

In this article we present adaptive numerical results of heat and mass transfer in fluidized beds using higher order time stepping methods. The model equations are strongly coupled and semi linear partial differential equations with boundary conditions. The invariant regions are presented for this model to check the solution bounds. These bounds gives the minimum and maximum values of solutions. The numerical discretization for the space using the finite element method is presented. For the time discretization higher order linearly implicit Runge-Kutta methods are used. These methods use the adaptive time step selection criteria to obtain the faster results.

The present article focuses on higher order and efficient numerical results for the solution of concentration and temperature distributions inside fluidized beds (FB) with liquid spray injection. The numerical results are tested with different time stepping methods for different spatial grid sizes. These methods shows very good improvement for this particular problem compared to the numerical results presented in Nagaiah [12]. The numerical results motivate us to proceed to more complicated three space dimensional simulations including exact mass balance equation for the liquid spray injection.

1 Introduction

The traditional importance of heat and mass transfer in chemistry, physics, and engineering, and the recent development of various reaction-diffusion processes in biology, ecology,

*nagaiah.chamakuri@uni-graz.at, Tel: +43 316 3805063, Fax: +43 316 3809815

†Gerald.Warnecke@ovgu.de, Tel: +49 391 6718587, Fax: +49 391 6718073

and biochemistry have led to many physically interesting and mathematically challenging problems using semi linear parabolic and hyperbolic equations. From the process engineering point of view, the fabrication and subsequent treatment of disperse products in fluidized beds is very important.

The modeling of heat and mass transfer in gas-solid-fluidized beds (FB) with spray injection is important for many applications. This process is widely used for the formation of particles from liquid solutions or suspensions as well as for the coating of particles with solid layers for the production of functional surfaces to enhance their handling properties, e.g. solvability properties, controlled release or protection from chemical reactions. Such a fluidized bed spray granulation (FBSG) system involves high heat and mass transfer and mixing properties, as well as the coupling of wetting, drying, particle enlargement, homogenization and separation processes. In FBSG, the liquid is sprayed with a nozzle as droplets on solid particles. The droplets are deposited on the particles and distributed through spreading. The solvent evaporates in the hot, unsaturated fluidization gas, thereby the solid grows in layers on the particle surface. The process conditions in the injection zone have a strong influence on the local particle volume concentrations, particle velocities, deposition of the liquid droplets and solidification of the solid content of the liquid and subsequent product quality.

When the injected liquid is sprayed on to the particles, this forms a spraying zone in the FB. Due to the higher liquid concentration near the mouth of the spraying jet, the model equations are more stiff in this region. And also when an arrangement of more spraying nozzles is used one needs robust numerical techniques to solve the system efficiently. The current work uses the standard Galerkin finite element method method for the spatial discretization. A system of ordinary differential equations (ODEs) is obtained after the space discretization. Due to the stiffness, we have mainly concentrated on implicit methods for solving these equations. To solve the ODEs, linearly implicit methods of Rosenbrock type [14] are employed which are constructed by calculating the inexact Jacobian. These methods offer several advantages. They completely avoid the solution of nonlinear equations, which means that no Newton iteration has to be controlled. More detailed expositions of these methods can be found in Hairer and Wanner [6], as well as Lang [9]. Also these methods are more suitable to use with adaptive time steps. An automatic step size selection procedure ensures that the step size is as large as possible while guaranteeing the desired precision, see Gustafsson et al. [5].

The motivation of this article is to present efficient and fast numerical results for the heat and mass transfer in fluidized beds. The presented numerical results based on the adaptive higher order numerical methods show faster computations than the previous numerical results which are based on the semi implicit Euler method. This motivates us to do more complicated numerical simulations in the three-space dimensions which thereby become feasible.

The organization of the current article is as follows: the governing equations are given briefly in the coming section. Then the model equation for the spraying liquid is presented. The invariant regions are presented for this current problem in the Section 3. The space and time discretizations are discussed in Section 4. Finally, the numerical results are presented

in the last section.

2 Governing equations and boundary conditions

The modeling of the problem is obtained by the balances of the mass and energy of the air, of the solid as well as of the liquid contained in the fluidized bed. The mathematical modeling of the problem can be found in our previous paper, see [12]. These equations are used in our numerical simulations. A similar type of modeling and experimental results can be found in [7, 8]. The balance inside the fluidized bed zone leads to a partial differential equation for each balance variable. The balance variables are functions of space and time. The following model equations are in Cartesian coordinates. We give the equations in two space dimensions.

Mass balance of air:

The mass balance of air in terms of air humidity is given as

$$\frac{\partial Y_A}{\partial t} = -W(\theta_A)\nabla \cdot Y_A + R_1(\theta_A)\phi(Y_{sat}(\theta_L) - Y_A), \tag{1}$$

where

$$W(\theta_A) = -\frac{\dot{m}_A}{m_A(\theta_A)}H_{fb}(\theta_A), \quad m_A(\theta_A) = \rho_A(\theta_A)\epsilon V_{fb}, \quad R_1(\theta_A) = \frac{A_P\beta(\theta_A)\rho_A(\theta_A)}{m_A(\theta_A)}.$$

Energy balance of air:

Heat transfer coefficients between the liquid film and air is α_{LA}, as well as particles and air α_{PA} are calculated according to [4]. Both heat transfer coefficients are assumed to be equal due to the same flow conditions, i.e. $\alpha_{PA} = \alpha_{LA} = \alpha$. The energy balance of the air, in terms of temperature of air is

$$\frac{\partial \theta_A}{\partial t} = -W(\theta_A)\frac{\partial \theta_A}{\partial z} - Q_1(Y_A, \theta_A)\{(1-\phi)(\theta_A - \theta_P) + \phi(\theta_A - \theta_L)\}, \tag{2}$$

where $Q_1 = \frac{\alpha(\theta_A)A_P}{m_A(\theta_A)(c_{pA}(\theta_A)+c_{pV}(\theta_A)Y_A)}$.

Mass balance of water:

The differential equation for the mass balance of the water in the form of degree of wetting

$$\frac{\partial \phi}{\partial t} = \nabla \cdot (D\nabla\phi) - R_2(\theta_A, \theta_L)\phi(Y_{sat}(\theta_L) - Y_A) + S_1(\theta_L)\dot{m}_{LV}, \tag{3}$$

where

$$R_2(\theta_A, \theta_L) = \frac{\beta(\theta_A)\rho_A(\theta_A)}{\rho_L(\theta_L)F}, \qquad S_1(\theta_L) = \frac{1}{A_p F \rho_L(\theta_L)}.$$

Energy balance of water:

The energy balance of water in terms of liquid temperature is

$$\frac{\partial(\phi\theta_L)}{\partial t} = \nabla\cdot(D\nabla(\phi\theta_L)) + Q_2(\theta_A,\theta_L)\{\phi(\theta_A-\theta_P) + f(\theta_A,\theta_L)\phi(\theta_P-\theta_L)\} + S_2(\theta_L)\dot{m}_{LV} - R_3(\theta_A,\theta_L)\phi(Y_{sat}(\theta_L)-Y_A)(\Delta h_V + c_{pV}(\theta_A)\theta_A), \tag{4}$$

where $Q_2(\theta_A,\theta_L) = \frac{\alpha(\theta_A)}{F\rho_L(\theta_L)c_L(\theta_L)}$, $R_3(\theta_A,\theta_L) = \frac{\beta(\theta_A)\rho_A(\theta_A)}{F\rho_L(\theta_L)c_L(\theta_L)}$, $S_2(\theta_L) = \frac{\theta_{L,in}}{A_P F\rho_L(\theta_L)}$.

Here a corrective factor $f(\theta_A,\theta_L)$ is defined, which specifies the ratio of the heat transport coefficient between the particle and the liquid film to the heat transfer coefficient in the fluidized bed, i.e.

$$f(\theta_A,\theta_L) = \frac{\alpha_{PL}}{\alpha}. \tag{5}$$

Energy balance of the particles:

Here the mass balance of the solid particles is not considered in our numerical simulations, because this equation is not coupled with the other balance quantities. It may be computed approximately. The enthalpy of the solids is obtained in the from of particle temperature,

$$\frac{\partial\theta_P}{\partial t} = \nabla\cdot(D\nabla\theta_P) + Q_3(\theta_A)\{(1-\phi)(\theta_A-\theta_P) - f(\theta_A,\theta_L)\phi(\theta_P-\theta_L)\}, \tag{6}$$

where $Q_3(\theta_A) = \frac{\alpha(\theta_A)A_P}{m_P c_{pP}}$.

2.1 Boundary conditions

The flow defined inside a fluidized bed region Ω should be a continuous vector field in $\bar{\Omega}$. The set $\bar{\Omega}$ denotes the closure of Ω, that is the union of the domain Ω with its boundary Γ: $\bar{\Omega} = \Omega\cup\Gamma$ and $\Gamma = \Gamma_D\cup\Gamma_N$. The vector $\underline{n}$ denotes the outward normal unit vector at the boundary Γ, λ characterizes the heat conduction coefficient on the apparatus surface and D is the dispersion matrix. The boundary of the fluidized bed zone is divided into 3 partial surfaces. The balance at each boundary surface delivers the corresponding boundary conditions of the partial differential equation system.

The bottom surface:

Vapor in the gas flow is transported from the air distributor at the bottom, to the top boundary of the fluidized bed zone. The humidity of air Y_A and the air temperature θ_A are determined at the boundary by the inflow of Y_A and inflow of θ_A

$$Y_{A|bot} = Y_{A,in} \quad \text{on} \quad \partial\Gamma_D\times[0,T],$$
$$\theta_{A|bot} = \theta_{A,in} \quad \text{on} \quad \partial\Gamma_D\times[0,T].$$

The boundary of the bed zone is not influenced by the particles and liquid flow. Therefore, the flow over the bottom boundary for ϕ, θ_L and θ_P is zero, i.e.

$$\begin{aligned} \underline{n} \cdot D\nabla\phi = 0 \quad &\text{on} \quad \partial\Gamma_N \times [0,T], \\ \underline{n} \cdot D\nabla\theta_L = 0 \quad &\text{on} \quad \partial\Gamma_N \times [0,T], \\ \underline{n} \cdot D\nabla\theta_P = 0 \quad &\text{on} \quad \partial\Gamma_N \times [0,T], \end{aligned}$$

where $Y_{A,in}, \theta_{A,in} \in \mathbb{R}$ are given constant data.

The apparatus wall and top surface:

For these surfaces Eq. (1) and Eq. (2) do not have a boundary conditions. The diffusive equations need a boundary condition. Here we assume that there is no flux of ϕ, θ_L and θ_P, i.e.

$$\begin{aligned} \underline{n} \cdot D\nabla\phi = 0 \quad &\text{on} \quad \partial\Gamma_N \times [0,T], \\ \underline{n} \cdot D\nabla\theta_L = 0 \quad &\text{on} \quad \partial\Gamma_N \times [0,T], \\ \underline{n} \cdot D\nabla\theta_P = 0 \quad &\text{on} \quad \partial\Gamma_N \times [0,T]. \end{aligned}$$

2.2 Liquid spray nozzle

The temperature and concentration distributions inside the fluidized bed are determined by the spatial distribution of the sprayed liquid and by liquid evaporation. The spraying area depends on the spraying angle and the penetration depth of the liquid droplets atomized by the nozzle, whereby the spraying angle is influenced by the nozzle characteristics. The penetration depth is determined by the intensity of the liquid drop deposition on the particles. The intensity of the drop deposition can be described by the *deposition efficiency* φ_{dep}. As an initial step, we assume that the drop deposition is constant for the calculation. The spray jet is considered to be a homogeneous conical drop flow. The model equation is derived based on the the distance from the nozzle and using other assumptions. Here we are not giving the full details of the derivation of this model, interested reader can be found more details in the thesis of Nagaiah [11].

Here is the model equations to approximate the mass balance of the spraying liquid,

$$\tilde{\kappa}(r,\vartheta) = \frac{\dot{m}_L}{\theta_{nozz}} \frac{\exp(\frac{-r}{s_{dr}})}{r s_{dr}}. \tag{7}$$

where $\tilde{\kappa}(r,\vartheta)$ is the drop concentration, $\dot{m}_L$ is the sprayed liquid mass per unit mass, θ_{nozz} is the angle of the spraying cone, r is the distance from the spray nozzle and s_{dr} is the average drop path length. The average drop path length is obtained according to Löffler [10] as

$$s_{dr} = \frac{2}{3} \frac{\epsilon}{1-\epsilon} \frac{d_p}{\varphi_{dep}}.$$

where d_p is the diameter of the particles and ϵ is porosity in the fluidized bed. In computations, we used the normalization to obtain the exact mass balance for the spraying liquid.

3 Invariant regions

In this section we give condition for an invariant region for the balance equations (1), (2), (3), (4) and (6). It provides a suitable theoretical foundation and frame work for studying the large time behavior of solutions.

Then we can write the set of Eqs. (1), (2), (3), (4) and (6), as

$$u_t = \mathbf{D}u_{xx} + \mathbf{M}u_x + \mathbf{F}(u) \tag{8}$$

with the initial data

$$u(x,0) = u_0(x), \quad x \in \Omega. \tag{9}$$

Definition 3.1. A closed subset $I \subset \mathbb{R}$ is called a *(positively) invariant region* for the local solution defined by system (8), (9), if any solution $u(x,t)$ having all of its boundary and initial values in I, satisfies $u(x,t) \in I$ for all $x \in \Omega$ and for all $t \in [0,T)$, see Smoller [15], page 199.

The invariant regions I we consider will be made up of the intersection of "half spaces", i.e. we consider regions I of the form

$$I = \cap_{i=1}^{m} \{u \in S : G_i(u) \leq 0\}, \tag{10}$$

where G_i are smooth real-valued functions defined on open subsets of S, and for each i, the gradient ∇G_i never vanishes.

Definition 3.2. The smooth function $G : \mathbb{R}^n \to \mathbb{R}$ is called *quasi-convex* at u if whenever the gradient vanishes, i.e. $\nabla G_u(u) = 0$, then the Hessian is non-negligible, i.e. $\mathcal{H}G_u(u,u) \geq 0$.

Theorem 3.1. *Let I be defined by (10), and suppose that I is an invariant region for (8), where $\mathbf{F} = \mathbf{F}(u,t)$ and $\mathbf{D}$ is a positive definite matrix. Then the following conditions hold at each point u_0 on ∂I, say, $G_i(u_0) = 0$:*

1. *∇G_i at u_0 is a left eigenvector of $\mathbf{D}(u_0, x)$, for all $x \in \omega$.*
2. *G_i is quasi-convex at u_0.*
3. *$\nabla G_i \cdot \mathbf{F} \leq 0$ for all $t \geq 0$.*

Proof. See Smoller [15], page 204. □

Lemma 3.2. *Let I is defined as in (10). Based on the above theorem the invariant regions for system Eqs. (1-6) are derived as following*

$$
\begin{aligned}
&Y_A \geq Y_{sat} - \frac{1}{R_3\phi(\Delta h_v + c_{st}\theta_A)}\Big\{Q_2\{\phi\theta_A + f_\alpha\phi\theta_P\} + S_2\dot{m}_{LV}\Big\} \quad at\ \theta_L = 0\,,\\
&Y_A \leq Y_{sat} - \frac{S_1}{R_2}\dot{m}_{LV} \quad at\ \phi = 1\,,\\
&Y_A \leq Y_{sat} - \frac{1}{R_3\phi(\Delta h_v + c_{st}\theta_A)}\Big\{Q_2\{\phi(\theta_A - \chi) + f_\alpha\phi(\theta_P - \chi)\} + S_2\dot{m}_{LV}\Big\}\ at\ \theta_L = \chi\,,\\
&\theta_L \leq \chi - \frac{1}{f_\alpha\phi}(1-\phi)(\theta_A - \chi) \quad at\ \theta_P = \chi\,.
\end{aligned}
$$

Under these conditions, the system (8) has an invariant region.

Proof. The detailed proof of these derived conditions can be found in the Ph.D thesis of Nagaiah [11]. □

4 Numerical discretization

The system of coupled nonlinear partial differential equations is valid in the fluidized bed interior Ω. We considered the domain $\Omega \subseteq \mathbb{R}^2$ is a rectangular domain. The state variables $Y_A(\underline{x},t), \phi(\underline{x},t)$, $\theta_A(\underline{x},t), \theta_L(\underline{x},t)$ and $\theta_P(\underline{x},t)$ are functions of space and time with values in $\Omega \times [0,T]$. In this section we describe the finite element method for solving the coupled convection-diffusion-reaction system. We use the method of lines approach. We will first consider a so-called *semi-discrete* analogue of the full system where we have discretized in space using the standard finite element method with piecewise linear continuous elements. To obtain a fully discrete problem we will then discretize in time also. Then the semi-discrete problem is an initial value problem for a system of ordinary differential equations. The formulation and subsequent discretization of such an integral form requires the definition of some function spaces and associated norms. Consider a spatial domain $\Omega \subset \mathbb{R}^2$ with piecewise smooth boundary Γ. We shall denote by $L^2(\Omega)$ the space of functions that are square-integrable over the domain Ω, see [1]. This space is equipped with the standard inner product

$$\langle u, v\rangle = \int_\Omega uv dx \quad \text{and} \quad \|u\|_0 = \langle u, u\rangle^{1/2}.$$

Next we define a particular class of Sobolev spaces, those of square integrable functions and derivatives.

$$H^1(\Omega) = \{v \in L^2(\Omega), \partial_i v \in L^2(\Omega), 1 \leq i \leq d\}.$$

And another class of functions which are square integrable, have square integrable first derivatives over the computational domain Ω, and vanish on the Dirichlet portion, Γ_D, of

the boundary. Those are defined as follows

$$V_D = \{v \in H^1(\Omega) |\ \ v \ = \ 0 \quad \text{on} \quad \Gamma_D\}.$$
$$V = \{u \in H^1(\Omega) |\ \ u \ = \ u_D \quad \text{on} \quad \Gamma_D\}.$$

Standard finite element texts, such as, for instance, [3], and [13] provide a detailed exposition of the mathematical concepts, which are the basis of the finite element method.

4.1 Semi discretization in space

The scalar partial differential equation can be written in following general form. Here we will show the space discretization for the scalar equation. Analogously we can extend the discretization to the system of partial differential equations

$$\begin{cases} \frac{\partial u(\mathbf{x},t)}{\partial t} - \nabla \cdot (a(\mathbf{x})\nabla u(\mathbf{x},t)) + b(\mathbf{x}) \cdot \nabla(u(\mathbf{x},t)) + s(u(\mathbf{x},t)) = f(\mathbf{x}) & \text{in } \ \Omega \times (0,T], \\ u(\mathbf{x},t) = u_0(\mathbf{x}) & \text{on } \ \Omega \times t = 0, \\ u(\mathbf{x},t) = u_D & \text{on } \ \Gamma_D \times [0,T], \\ \underline{n} \cdot a(\mathbf{x})\nabla u = 0 & \text{on } \ \Gamma_N \times [0,T], \end{cases}$$

where u is a unknown, $a(\mathbf{x}) > 0$ is the diffusion matrix, $b(\mathbf{x})$ is the convection velocity and f is source function. The function u_D denotes the prescribed values of u on the Dirichlet portion Γ_D of the boundary, while the diffusive flux on the Neumann portion Γ_N is zero.

The discretization process using the finite element method is based on a reformulation of the given differential equation in more general, *variational formulation*. Multiplying above equation for a given time t by $v \in V_D$, integrating over Ω and using Green's formula, we get the following variational formulation:

Find $u \in V$ s.t: for each $t \in I = [0,T]$

$$\begin{cases} \langle \frac{\partial u}{\partial t}, v\rangle + \langle a(\mathbf{x})\nabla u, \nabla v\rangle + \langle b(\mathbf{x}) \cdot u, v\rangle + \langle s(u), v\rangle = \langle f, v\rangle & \text{for all } \ v \in V_D \\ u(\mathbf{x},t) = u_0(\mathbf{x}) & \text{on } \ \Omega \times t = 0 \\ u(\mathbf{x},t) = u_D & \text{on } \ \Gamma_D \times [0,T] \end{cases}$$

Let $V_h \subset V$ and $V_{D_h} \subset V_D$ be finite dimensional subspaces. Due to the presence of Dirichlet boundary conditions, a distinction must be made between the number of nodal points N of the discretized domain and the number of nodal unknowns, that is the number of equations N_e of the system. Furthermore, we denote by $N_D \subset N$ the subset of nodes on which the Dirichlet condition is given and replacing the space V by the finite dimensional subspace V_{D_h}. The weighting functions $v_h \in V_{D_h}$ vanish on the Γ_D. And the subspace V_h is spanned by the basis functions $\{w_i | i \in N \setminus N_D\}$. Specifically we take continuous functions that are piecewise linear on a quasi-uniform triangulation. As basis functions w_i we take the shape functions also known as hat functions. We approximate the solution u_h using the basis functions

$$u_h(t,\mathbf{x}) = \sum_{i \in N \setminus N_D} u_i(t) w_i(\mathbf{x}) + \sum_{i \in N_D} u_D w_i(\mathbf{x}) \tag{11}$$

i.e, each $u_h \in V_h$ can be written in a unique way as a linear combination of the basis functions w_i and time dependent coefficients. Moreover, the test functions v_h are defined such that

$$v_h \in V_h := \text{span}\{w_i\} \quad \text{where } i \in N \setminus N_D. \tag{12}$$

Thus, after substitution of Eq. (11) into the semi discretization, and testing with each of the basis functions, we get a system of ordinary differential equations in matrix form

$$M\dot{\mathsf{u}} + A\mathsf{u} + B\mathsf{u} + \mathsf{s}(\mathsf{u}) = \mathsf{f} \tag{13}$$

where M is the mass matrix, A is the stiffness matrix. The matrices are defined as follows,

$$\begin{array}{ll} M = \langle w_i, w_j \rangle, & A = \langle a(\underline{x})\nabla w_i, \nabla w_j \rangle \\ B = \langle b(\mathbf{x}) \cdot \nabla w_i, w_j \rangle, & \mathsf{s}(\mathsf{u}) = \langle s(\sum_{i=1}^{N} u_i(t) w_i(\mathbf{x})), w_j \rangle. \end{array}$$

We can apply the analogous spatial discretization to Eqs. (1), (2), (3), (4) and (6), then we get the $5 \cdot N$ ordinary differential equation system as follows:

$$\mathbf{M}\dot{\mathbf{u}} + \mathbf{A}\mathbf{u} + \mathbf{B}\mathbf{u} + \mathbf{s}(\mathbf{u}) = \mathbf{f} \tag{14}$$

where $\mathbf{M} = \text{diag}(M, M, M, M, M)$, $\mathbf{A} = \text{diag}(0, 0, A, A, A)$, $\mathbf{B} = \text{diag}(B, B, 0, 0, 0)$ and $\mathbf{s}(\mathbf{u})$ is a $5 \cdot N \times 1$ vector depending on the reaction terms and $\mathbf{f}$ is a $5 \cdot N \times 1$ vector that depends on the right hand side of the equations.

4.2 Linearly implicit Runge-Kutta time stepping methods

The matrix system Eq. (14) has to undergo a discretization in time after the discretization in space described above. The ordinary differential equation system, acquired from the semi discretization in space is solved numerically with finite difference methods. We considered the ODE problem

$$\mathbf{M}\frac{\partial \mathbf{u}}{\partial t} = \mathbf{F}(\mathbf{u}), \qquad \mathbf{u}(t^0) = \mathbf{u^0}. \tag{15}$$

To start with, we partition the time $[0, T]$ into discrete steps

$$0 = t^0, t^1, \ldots, t^n = T\,,$$

that are not necessarily equidistant. The notation for time step is $\tau^i = t^{i+1} - t^i$ and $\mathbf{u}^i$ to be the numerical solution at time t^i. For the time discretization we used a Rosenbrock method. Rosenbrock methods belong to a large class of methods which try to avoid nonlinear systems and replace them by a sequence of linear systems. For computation an s-stage *Rosenbrock*

method of order p with embedding of order $\hat{p} \neq p$ has the form

$$(\frac{1}{\tau^i \gamma}\mathbf{M} - \mathbf{J})\mathbf{k}_j = \mathbf{F}(t^i + \tau^i \alpha_j, \mathbf{u}^i + \tau^i \sum_{l=1}^{j-1} a_{jl}\mathbf{k}_l) - \mathbf{M}\sum_{l=1}^{j-1} \frac{c_{lj}}{\tau^i}\mathbf{k}_l\,, \quad j = 1, \ldots, s\,, \tag{16}$$

$$\mathbf{u}^{i+1} = \mathbf{u}^i + \sum_{l=1}^{s} m_l \mathbf{k}_l\,, \tag{17}$$

$$\hat{\mathbf{u}}^{i+1} = \mathbf{u}^i + \sum_{l=1}^{s} \hat{m}_l \mathbf{k}_l\,. \tag{18}$$

The method coefficients $\gamma, \alpha_j, a_{jl}, c_{jl}, m_l$, and $\hat{m}_l$ are chosen such a way that some order conditions are fulfilled to obtain a sufficient consistency order. A derivation of these conditions with Butcher series can be found in [6]. We assume $p > \hat{p}$ which is reasonable since one would prefer to continue the integration with the higher order solution $\mathbf{u}$. The Jacobian is given as $\mathbf{J} = \frac{\partial \mathbf{F}(\mathbf{u}_h(t^i))}{\partial \mathbf{u}_h}$ and we used the exact Jacobian in computations.

After the i-th integration step the value $\epsilon^{i+1} = \|\mathbf{u}^{i+1} - \hat{\mathbf{u}}^{i+1}\|$ is taken as an estimator of the local temporal error. We use the scaled norm given by

$$\|\mathbf{v}\| := \|\mathbf{v}\|/\sqrt{N}\,, \tag{19}$$

where N is the length of vector $\mathbf{v}$. A new time step τ_{new}, see Gustafsson et al. [5], is computed by

$$\bar{\tau} := \beta \frac{\tau^i}{\tau^{i-1}} \left(\frac{TOL_t}{\epsilon^{i+1}}\right)^{\frac{p_2}{p}} \left(\frac{\epsilon^i}{\epsilon^{i+1}}\right)^{\frac{p_1}{p}} \tau^i, \quad \tau_{\text{new}} = \begin{cases} \beta_{\max}\tau^i, & \bar{\tau} > \beta_{\max}\tau^i, \\ \beta_{\min}\tau^i, & \bar{\tau} < \beta_{\min}\tau^i, \\ \bar{\tau}, & \text{otherwise.} \end{cases} \tag{20}$$

The parameter $\beta > 0$ is safety factor. The factors $\beta_{\min}$ and $\beta_{\max}$ restrict time step jumps. In our computations we have chosen the parameters $p_1 = 1$ and $p_2 = 1$. If $\epsilon < TOL_t$ we proceed to the next time step, otherwise the time step has to be shortened and repeated.

In computations we used the ROS2, ROS3P, ROWDA3, RODASP methods which have 2 or 3 or 4 internal stages to solve. Finally, after time discretization, we get a system of algebraic equations in each stage. For solving the system in each stage we used the BiCGSTAB method [16] with the ILU preconditioner.

5 Numerical results

The two space dimensional transient numerical simulations of balance equations are presented in this section. The fluidized bed zone is represented by a rectangular geometry in the numerical simulation. The numerical implementation of this problem is realized with the FE simulation package called DUNE, see [2], which is a public domain software and completely written in C++. All the numerical computations presented in this article were performed on Linux PC, Intel(R) Core(TM)2 Duo, with 3.5GB RAM, 2.6 GHz processor, gcc-4.2.1 compiler.

5.1 Numerical results for the balance quantities

We considered as computational domain $\Omega = [0, 0] \times [0.4, 0.2]$, i.e. the cross section of the apparatus is 0.4 m and the height of the fluidized bed is 0.2 m. The tolerance for the time step selection was taken to be 10^{-4}.

In this subsection we present the time dependent numerical solution of the air humidity, air temperature, degree of wetting, liquid film temperature and particle temperature, taking into account a liquid spray nozzle injection. And we give the numerical solution at the particular time $t = 400\ s$. We describe non-ideal particle mixing and thus non-uniform liquid distribution by assuming axial and radial particle dispersion coefficients.

We assume that the spraying has occurred at the top surface of the apparatus and the position of the nozzle is fixed at $(0.2, 0.2)$ and with a spraying angle of $60°$. For simulations we used the initial parameters as listed in Table 3, whereby a constant wall temperature is assumed. For the simulations the deposition efficiency is kept constant with $\phi_{dep} = 20\%$. According to Eq. (7), the representation of the mass flow of the liquid shows a complete deposition of the liquid droplets onto the particles after some centimeters near the nozzle region. This means that the evaporation also takes place primarily in the nozzle region.

The sprayed liquid is distributed over the domain, with a spraying rate $\dot{m}_L = 5.9\ kg/h$. Here we consider that the sprayed liquid to be water. For simulations, we assume that the wall temperature is constant. All parameters used for the simulation are listed in Table 3. We can observe from the left hand side of Figure 1 that the air humidity increases rapidly in the initial period. When the liquid distribution starts at the top the domain, the air humidity increases suddenly at the outlet, and then increases slowly until it reaches the stationary solution. Thereby the steady-state is reached after 200 seconds.

The particle temperature decreases slightly slower than the air temperature because of the particle heat capacity. During stationary operation it lies somewhat under the air temperature, see the Figure 3. At initial time $t = 0$ the average of degree of wetting is 10^{-8}. When the simulation starts it increases sharply to 0.30% and thereafter increases steadily towards the final value 0.35%. This is due to the fact that the temperature of the liquid is 20 $°C$ and so the liquid film temperature sinks where energy is absorbed from the particles and increases where the energy is emitted, see Figure 2. Here we cannot show the time dependent behavior of all the parameters, we show only the behavior of the air humidity at different time levels, see Figure 4. The invariant regions, which were presented in section 3, are validated for these computations.

5.2 Convergence tests for the different numerical methods

In this subsection, first we present numerical results based on the experimental order of convergence for the implicit Euler method. In Table 1 we give the experimental order of convergence of the semi implicit Euler method for the balance variable of air humidity. The first column indicates the mesh size and the second column shows the L^2 error of the mesh sizes h and $h/2$. The last column represents the experimental order of convergence

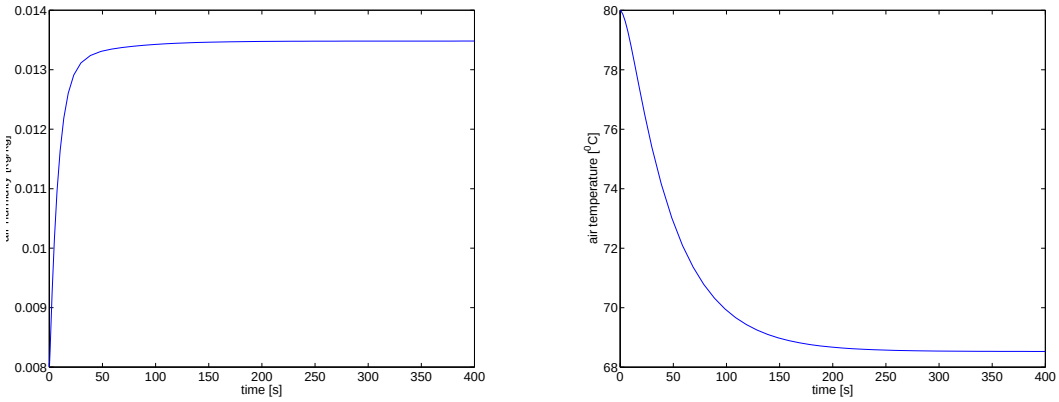

Figure 1: The outlet value of the air humidity and air temperature over the time.

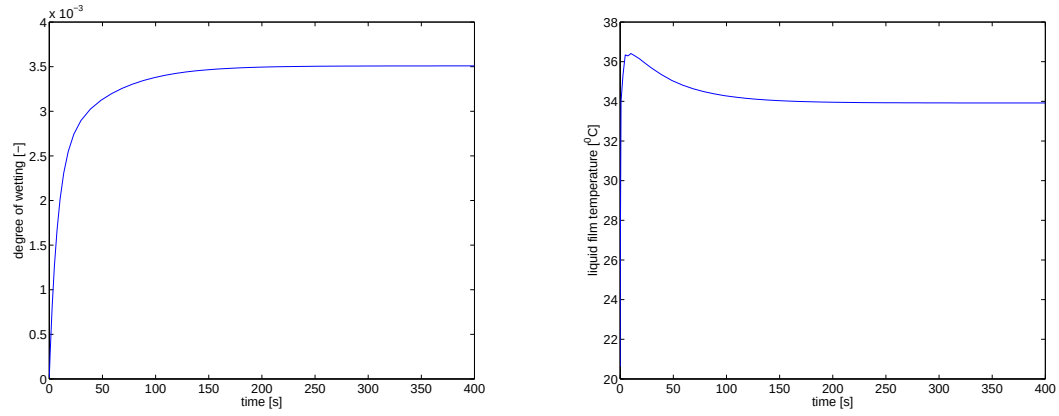

Figure 2: Outlet value of the degree of wetting and liquid film temperature over the time.

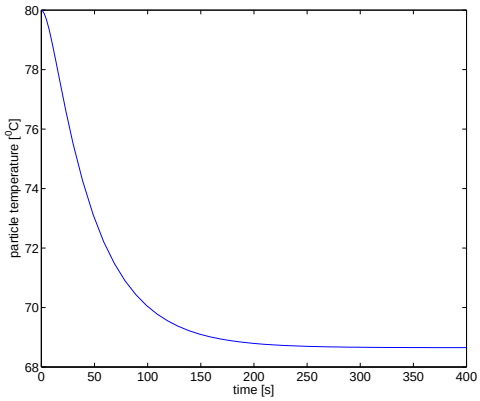

Figure 3: Outlet value of the particle temperature over the time.

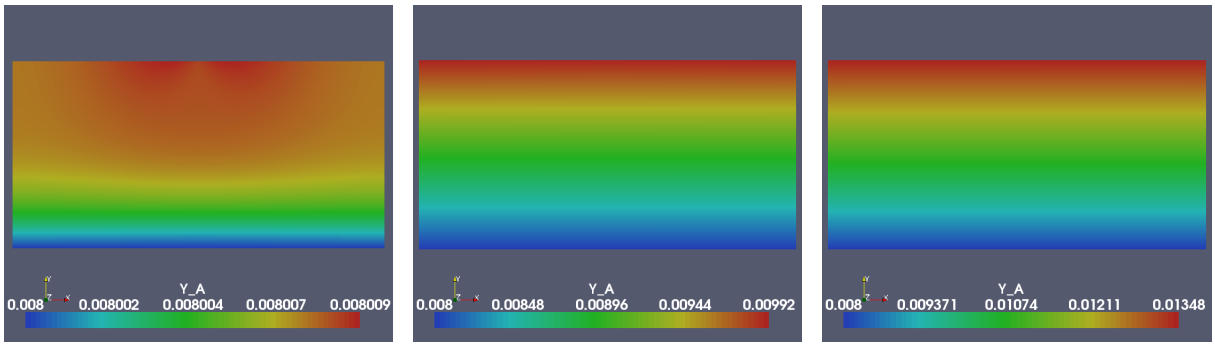

Figure 4: Solution of the air humidity at time $t = 0.1\ s,\ 4.03\ s,\ 400\ s$.

mesh size	Semi implicit Euler		ROS2	
	$\|u_{h/2} - u_h\|_{L^\infty}$	EOC	$\|u_{h/2} - u_h\|_{L^\infty}$	EOC
17×17	-	-	-	-
34×34	0.02468235	0.9521690121	7.0000000000006e-06	1.0848888975
68×68	0.04775490	0.9781248865	3.3000000000121e-06	1.7224660244
136×136	0.09407254	-	1.0000000000010e-06	1.7369655941
272×272	-	-	2.9999999999995e-07	-

Table 1: Experimental order of convergence of the air humidity at the stationary solution for the semi implicit Euler method and ROS2 method.

(EOC), which is defined with respect to the L^p-norm as

$$\text{EOC} = \ln\left[\frac{\|u_{h/2} - u_h\|_{L^p}}{\|u_{h/4} - u_{h/2}\|_{L^p}}\right] / \ln(2), \qquad \text{for } (1 \leq p \leq \infty). \tag{21}$$

We can observe that the EOC is achieved successfully almost at the expected value 1 for semi implicit Euler method. This result demonstrates that the method has a practical convergence order that agrees with the theoretical considerations. The EOC for the ROS2 method is shown in Table 1 and we can observe that this method has order 1.7369655941 in the case of fine mesh. This is satisfactory, though theoretically we expect the order.

The EOC is shown in Table 2 in the case of 3 stage linearly implicit methods, ROS3p and ROWDA3 methods. Here we can observe that both methods have same EOC, which is 1.8744691179, for fine meshes. This order is little better than for the 2-stage method. The EOC for the RODAS method has also achieved the same value as ROS3p and ROWDA3 method.

The comparison between the different linearly implicit methods and the semi implicit Euler method are presented in Figure 5. In this case we used the fixed time step for the semi implicit Euler method and adaptive time step for the linearly implicit methods. Here the outlet air humidity is plotted at left and the outlet value of the air temperature plotted at right up to a simulation time of 100 seconds only for a better view of the transition period. Here we can observe that all the time stepping methods have the same convergence rate

mesh size	ROS3p		ROWDA3	
	$\|\|u_{h/2} - u_h\|\|_{L^\infty}$	EOC	$\|\|u_{h/2} - u_h\|\|_{L^\infty}$	EOC
17×17	-	-	-	-
34×34	7.099999999999e-06	1.1053530001	7.099999999999e-06	1.1053530001
68×68	3.300000000001e-06	1.5849625007	3.300000000001e-06	1.5849625007
136×136	1.100000000004e-06	1.8744691179	1.100000000004e-06	1.8744691179
272×272	3.000000000016e-07	-	3.000000000016e-07	-

Table 2: Experimental order of convergence of the air humidity at the stationary solution for the semi implicit Euler method and ROS2 method.

to reach the same stationary solution in the case of air humidity balance variable. But in the case of the air temperature balance variable they reached to slight different stationary solution at the end of simulation. For this calculation the CPU time for the ROS2 is 73.2086 seconds, ROS3P is 70.4724 seconds, ROWDA3 is 69.9524 seconds while RODAS is 84.0573 seconds. One can observe that ROWDA3 method takes less CPU time compared to other methods.

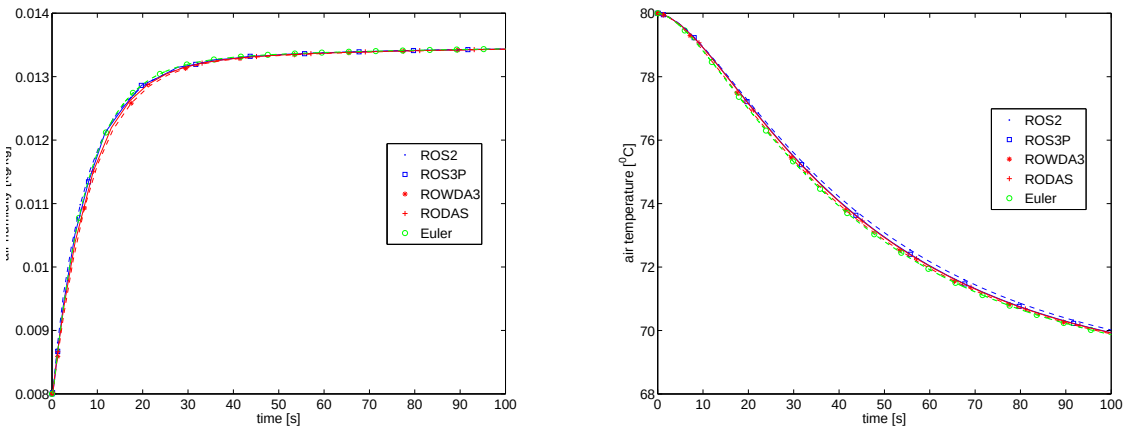

Figure 5: Outlet value of the air humidity and air temperature over the time for different time stepping methods.

The accepted time steps for different methods are presented at the left hand side of Figure 6. The maximum time step is restricted 10 s and the ROWDA3 method takes fewer time steps to reach the stationary solution. This suggests that ROWDA3 method is very suitable for these calculations.

The convergence test for the different meshes using the ROWDA3 method is presented at the right hand side of Figure 7. Clearly we can see that for all the meshes the outlet value of air humidity reached the same value and there is a small difference in the case of the outlet value of air temperature. This suggests to take a 100×100 mesh for the

computations to get accurate numerical results.

6 Conclusions and outlook

In the present paper the mathematical solution of the continuum model was approximated by using a higher order time stepping methods in order to improve the numerical efficiency. The invariant regions are shown for this particular problem to find the solution bounds on the numerical simulations. The time-dependent two-dimensional distributions of air humidity, air temperature, particle wetting, liquid film temperature and particle temperature were simulated, which show the influence of the nozzle and the almost isothermal behavior with the good mixing conditions of the fluidized beds. The numerical results are tested with different grid arrangements which shows the numerical convergence of the computer implementation. The numerical results are tested with different time stepping methods which shows a good improvement over the first order Euler semi implicit methods. Finally, the presented numerical results show that adaptive higher order time stepping methods are more efficient to consider for this problem. Further, motivated by form these results we intend to do real 3D simulations with considering the non ideal particle mixing, which has more influence on the mass and energy of particles as well as liquid thermal conditions. Also, we would like to then consider the exact mass balance equation which is a typically hyperbolic equation. It is challenging to to solve numerically the coupled hyperbolic and parabolic equation system in three space dimensions.

Acknowledgement

This work was supported by the Graduiertenkolleg-828, "Micro-Macro-Interactions in Structured Media and Particles Systems", Otto-von-Guericke-University Magdeburg. The authors gratefully acknowledge for funding through this PhD program. We also thank the DUNE developer team, see e.g. [2], for making their software available to us.

References

[1] Adams. *Sobolev Spaces*. Cambridge University Press, 2001.

[2] P. Bastian, M. Blatt, A. Dedner, C. Engwer, R. Klöfkorn, R. Kornhuber, M. Ohlberger, and O. Sander. A generic grid interface for parallel and adaptive scientific computing. part II: Implementation and tests in dune. *Matheon preprint*, 2007.

[3] D. Braess. *Finite elements: Theory, Fast Solvers, and Applications in Solid Mechanics*. Cambridge University Press, 2001.

[4] V. Gnielinski. Wärme- und Steffübertragung in Festbetten. *Chem.-Ing.-Tech.*, 52:228–236, 1980.

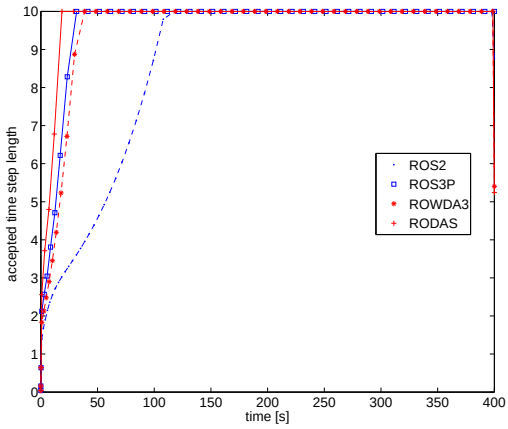

Figure 6: The accepted time steps over the time for different time stepping methods.

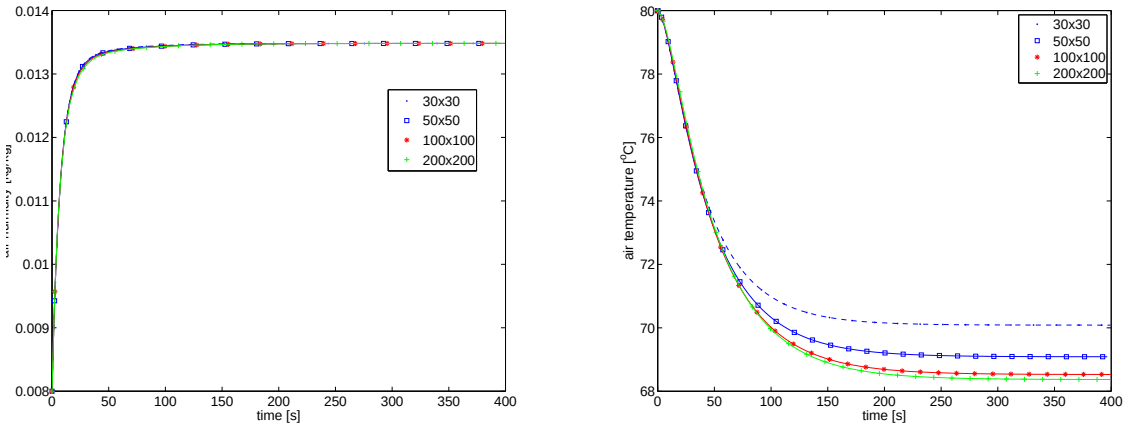

Figure 7: Outlet value of the air humidity over the time for ROWDA3 method with different grid sizes.

[5] K. Gustafsson, M. Lundh, and G. Söderlind. A pi stepsize control for the numerical solution of ordinary differential equations. *BIT*, 28(2):270–287, 1988.

[6] E. Hairer and G. Wanner. *Solving Ordinary Differential Equations II.* Springer Series in Computational Mathematics, 1991.

[7] S. Heinrich, J. Blumschein, M. Henneberg, M. Ihlow, M. Peglow, and L. Mörl. Study of multi-dimensional temperature and concentration distributions in liquid sprayed fluidized beds. *Chem. Eng. Sci.*, 55:5135–5160, 2003.

[8] M. Henneberg. *Untersuchung des Flüssigkeitseintrages auf die Temperaturverteilung in Gas/Feststoff-Wirbelschichten.* PhD thesis, Otto-von-Guericke-University Magdeburg, 2004.

[9] J. Lang. *Adaptive Multilevel Solution of Nonlinear Parabolic PDE Systems*, volume 16 of *Lecture Notes in Computational Science and Engineering.* Springer-Verlag, Berlin, 2001.

[10] F. Löffler. *Staubabscheiden.* Thieme, Stuttgart, 1988.

[11] Ch. Nagaiah. *Adaptive numerical simulation of reaction-diffusion systems.* PhD thesis, Otto-von-Guericke-University Magdeburg, Germany, 2007.

[12] Ch. Nagaiah, G. Warnecke, S. Heinrich, and M. Peglow. Numerical simulation of temperature and concentration distributions in fluidized beds with liquid injection. *Chem. Eng. Sci*, 62:1567–1590, 2007.

[13] A. Quarteroni and A. Valli. *Numerical Approximation of Partial Differential Equations.* Springer Series in Computational Mathematics, 1994.

[14] H. H. Rosenbrock. Some general implicit processes for the numerical solution of differential equations. *Computer J.*, 5:329–330, 1963.

[15] J. Smoller. *Shock Waves and Reaction-Diffusion Equations.* Springer-Verlag, New York, 1995.

[16] H. A. van der Vorst. Bi-CGSTAB: A fast and smoothly converging variant of bi-cg for the solution of nonsymmetric linear systems. *SIAM J. Sci. Stat. Comput.*, 13:631–644, 1994.

A Simulation Parameters

Fluidized bed parameters			
width	L	0.4	m
height	H_{fb}	0.2	m
Bed material (glass spheres)			
total mass	m_P	18	kg
diameter	d_P	1.16	mm
density	ρ_P	2471	kg/m^3
specific heat capacity	c_P	750	J/(kg K)
thermal conductivity	λ_P	0.8	W/(m K)
Fluidization air			
mass flow rate	$\dot{m}_A$	0.304	kg/s
inlet humidity	$Y_{A,in}$	0.008	kg/kg
inlet temperature	$\theta_{A,in}$	80	° C
Liquid spraying			
spraying rate (source flow)	$\dot{m}_L$	6	kg/h
liquid inlet temperature	$\theta_{L,in}$	20	°C
Other parameters			
apparatus wall temperature	θ_W	75	°C
liquid film thickness	F	100	μm
heat transfer ratio	f	1	-
Initial parameters for the simulation			
air humidity	$Y_{A,0}$	0.008	kg/kg
air temperature	$\theta_{A,0}$	80	°C
degree of wetting	ϕ_0	1e-8	-
liquid film temperature	$\theta_{L,0}$	20	°C
particle temperature	$\theta_{P,0}$	80	°C

Table 3: Parameters values used for simulations in 2D